Anisotropy of electronic stopping power in graphite

Jessica Halliday [1] and Emilio Artacho[1,2,3]

[1]*Theory of Condensed Matter, Cavendish Laboratory, University of Cambridge, J. J. Thomson Ave, Cambridge CB3 0HE, United Kingdom*
[2]*CIC Nanogune and DIPC, Tolosa Hiribidea 76, 20018 San Sebastian, Spain*
[3]*Ikerbasque, Basque Foundation for Science, 48011 Bilbao, Spain*

The rate of energy transfer from ion projectiles onto the electrons of a solid target is hard to determine experimentally in the velocity regime between the adiabatic limit and the Bragg peak. First-principles simulations have lately offered relevant new insights and quantitative information for prototypical homogeneous materials. Here, we study the influence of structural anisotropy on electronic stopping power with time-dependent density functional theory simulations of a hydrogen projectile in graphite. The projectile traveled at a range of angles and impact parameters for velocities between 0.1 and 1.4 a.u., and the electronic stopping power was calculated for each simulation. After validation with average experimental data, the anisotropic crystal structure was found to have a strong influence on the stopping power, with a difference between simulations parallel and perpendicular to the graphite plane of up to 25%, more anisotropic than expected based on previous work. The velocity dependence at low velocity displays clear linear behavior in general, except for projectiles traveling perpendicular to graphitic layers, for which a thresholdlike behavior is obtained. For projectiles traveling along graphitic planes, metallic behavior is observed with a change of slope when the projectile velocity reaches the Fermi velocity of the electrons.

I. INTRODUCTION

Stopping power is the rate of energy loss along the path of a charged particle as it passes through matter. Stopping power is of interest in a wide range of areas, from nuclear power generation to medical applications [1,2]. Two mechanisms of energy loss are involved: nuclear stopping, due to the interaction of the projectile with the nuclei of the target, and electronic stopping, from the interaction of the projectile with the electrons of the target. This work focuses on the electronic stopping power (S_e), which dominates at high projectile velocities.

Most of modern electronics is based on materials and heterostructures grown along well-controlled crystalline directions, a trend that appears to continue in the brave new world of two-dimensional materials, heterostructures, and devices based on them. A good characterization of the orientation dependence of radiation effects would appear quite relevant for ascertaining on resilience of such devices. Of particular interest is the velocity regime in which projectiles are fast enough for nonadiabatic effects to be important, but not so fast so as to become insensitive the structure, pointing to the scale of a few tenths of an atomic unit of velocity (1 a.u.= $c/137$). Previous studies in various materials have investigated anisotropy in S_e in thin films, particularly at higher energies [3–5] However, knowledge of the effect of structural anisotropy at velocities of a few tenths of a.u. is still very limited given the difficulties in obtaining experimental information in this range [6–10].

Experimentally, S_e is difficult to measure directly, particularly at low velocities where nuclear stopping is also significant; simulations, however, allow S_e to be directly accessed. Echenique *et al.* [11,12] used density functional theory to calculate electronic stopping power in jellium, capturing nonlinear effects and replicating experimental results not captured in linear-response theory calculations [13,14], also giving rise to derived simulations, including the use of first-principles techniques for the indirect calculation of S_e (for reviews, see [15,16]). Direct, real-time simulations of the electronic stopping process have also been performed during the last decade using a time-dependent tight-binding description of the electronic structure and dynamics, coupled to nuclear dynamics within an Ehrenfest approach [17,18], providing interesting and rich qualitative insights, especially powerful given the large system size and long timescale affordable with an empirical tight-binding scheme. In recent years time-dependent density functional theory (TDDFT) has been used to investigate stopping power from first principles in bulk materials of different kinds (metals, semiconductors, insulators) [19–31]. First-principles simulation of electronic stopping has successfully reproduced many experimental features not captured by other theoretical or simulation methods.

A prototypical material with a highly anisotropic layered structure is graphite, composed of weakly bonded layers of strongly hexagonally bonded carbon atoms, resulting in a high degree of inhomogeneity in many properties [32]. A major use of graphite is as a moderator in the nuclear power industry, to absorb and slow down the neutrons generated by the nuclear fission processes, in order to control the rate of fission within a nuclear reactor. The stopping power of graphite is thus of intrinsic interest, in addition to its position as a simple and strongly anisotropic material, and was therefore chosen as the target material in this work. The velocity dependence of S_e is

addressed in the work, with an emphasis on its variation with trajectory.

A previous work on anisotropy of stopping power in graphite is a theoretical study by Crawford [9], using linear-response theory based on the Cazaux model [33] for the optical constants of graphite parallel and perpendicular to the graphitic layers. Crawford's work calculated, for higher-energy projectiles, a similar relationship between the incident angle of the projectile and the S_e as this work. They found a small anisotropy of S_e, with a variability of around 10% for projectile velocities between 2 and 20 a.u.. More recent work by Shukri, Bruneval, and Reining [10] used linear-response TDDFT to predict the random electronic stopping power in various materials. They found a similar small anisotropy of up to 3% between the S_e along the in-plane and out-of-plane axes of graphite, for velocities between 0 and 4 a.u. Previous experimental work by Yagi *et al.* [34] was unable to direct projectiles between the graphitic layers, illustrating the usefulness of simulations to investigate the structural anisotropy of S_e.

II. METHOD

A. Simulation details

Simulations were carried out using the real-time TDDFT implementation [35,36] of the SIESTA method [37,38]. The Kohn-Sham orbitals are expanded in a finite basis set of numerical atomic orbitals, with the valence electrons of graphite and the projectile represented by a double-ζ polarized basis set. The core electrons have been replaced by norm-conserving pseudopotentials using the Troullier-Martins scheme [39,40]. Core electrons are known not to interact in stopping processes at low velocities [10,41]. The details of both the basis set and the pseudopotentials are specified in the Appendix. The local density approximation (LDA) was used for the exchange-correlation functional evaluation using the Ceperley-Alder results for the homogeneous electron liquid [42], in the parametrization of Perdew and Zunger [43], considering adiabatic time dependence of the exchange-correlation functional.

The ground state of the system is calculated with the projectile stationary at its initial position in the graphite box. Subsequent TDDFT simulations evolve the electronic wave functions according to the time-dependent Kohn-Sham equation [44,45] as the projectile moves at a constant velocity through the box. The forces on all atoms are held as zero throughout the time-dependent simulation, so that energy transfer only takes place through inelastic scattering to the system electrons. This prevents any contribution from nuclear stopping and enables the S_e to be directly calculated at a single velocity for each simulation. The electronic stopping is the average gradient of the total energy of the electronic system as a function of the path length of the projectile [27]. The error bars in the S_e presented in the figures refer to uncertainty in fitting to the slope.

Projectiles moved the full length of the simulation cell, 13.4 Å. Simulations were carried out using projectiles with velocities between 0.1 and 1.4 a.u. [46]. The time-dependent Kohn-Sham equations were integrated using a Crank-Nicholson integrator as in Ref. [35] adapted to the
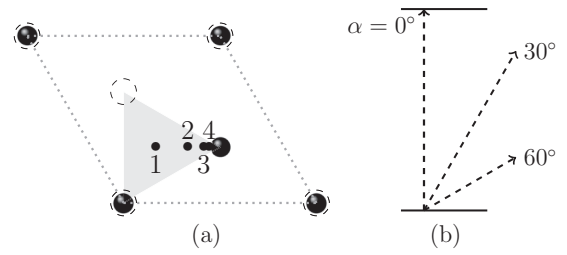

FIG. 1. (a) Graphite unit cell showing the projectile initial positions 1–4 and (b) trajectories for simulations of projectiles moving out of the plane of graphitic layers. The shaded triangle in (a) is the region of crystallographically unique positions. α is the angle of the trajectory from the graphite c axis, with $\alpha = 0°$ perpendicular to the graphitic planes.

changing basis and Hilbert space by using a Löwdin transformation as proposed by Sankey and Tomkoff [47] and analyzed in Ref. [48]. See the Appendix for further details of convergence testing.

B. Simulation trajectories

Simulations were run with a combination of the following parameters: the velocity of the projectile varied between 0.1 and 1.4 a.u., and the initial angle of the projectile relative to the c axis of the graphite, α, varied between 0° and 90° as shown in Fig. 1. For simulations of projectiles moving parallel to the graphitic layers, the projectiles moved at an angle β relative to the a axis, at 0° and 30°, with checks at 60° and 90° as shown in Fig. 2, and moving at distances of $\frac{1}{2}$, $\frac{1}{4}$, $\frac{1}{8}$, and $\frac{1}{16}$ of the spacing between the layers from the closest graphitic layer, as shown in Fig. 2.

Concerning the charge state of the projectile, previous TDDFT work on electronic stopping has been carried out with both ions and atoms [19,23,24,27]. In this type of simulation, the use of a proton or a H atom only changes the simulation by one electron in the supercell (out of 129). The extent to which the proton drags an electron in its wake is defined dynamically, and the established stationary state is independent of the initial charge state of the projectile. After the initial transient, essentially the same state evolves regardless of whether it was initially H^+ or H, in comparison with other methods in which the charge state is defined by hand [15]. The calculations presented here had 129 electrons in the simulation box, thereby defining an overall neutral
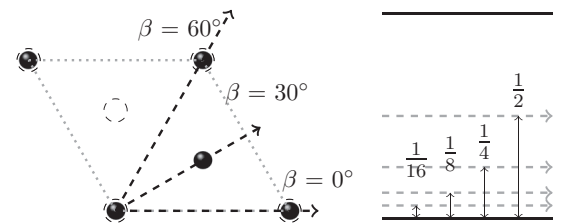

FIG. 2. (a) Graphite unit cell showing the projectile trajectories for simulations of projectiles moving parallel to the graphitic layers ($\alpha = 90°$). β is the angle of the trajectory from the a axis of the unit cell. $\beta = 0°$ and 60° are crystallographically equivalent. (b) Distance of projectile trajectories from the graphitic planes.
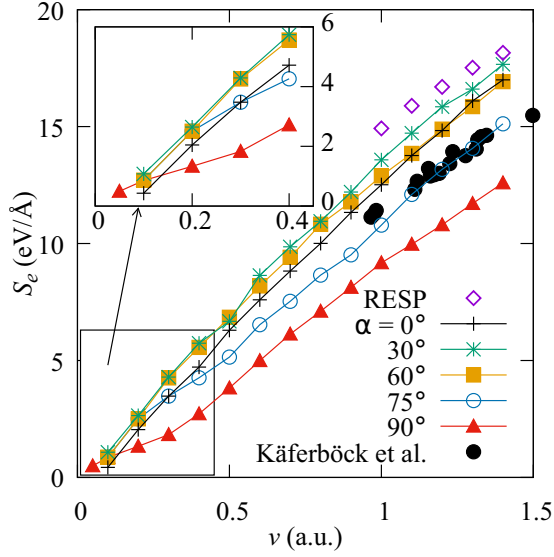
FIG. 3. Electronic stopping power for a proton shooting through graphite at different angles relative to the graphite c axis. The filled circle depicts the experimental data from the work by Käferböck *et al.* [6]. The uncertainty in each data point is ± 0.6 eV/Å. RESP is the random electronic stopping power for $\alpha = 90°$, averaged over all impact parameters simulated for comparison with Ref. [10].

system. The calculations were spin polarized due to the odd number of electrons in the system.

III. RESULTS AND DISCUSSION

A. Validation

In order to validate the simulations, the results are compared in Fig. 3 with experimental data from work by Käferböck *et al.* [6]. In the velocity range covered by the experimental data, electronic stopping dominates the overall stopping power, so the simulations of electronic stopping are directly comparable to the Käferböck data. The Rutherford backscattering experiment used protons with an energy of between 20 and 80 keV, corresponding to projectile velocities between 1 and 1.7 a.u., with a target of highly ordered pyrolytic graphite, although they did not provide angle resolution for the measured S_e. They consider ion trajectories in all directions.

In Fig. 3, the agreement between experiment and theory is clear, with the experimental observations lying within the simulation range defined by different trajectories. The experimental stopping power is closest to that of the higher-angle simulations $\alpha = 60°–75°$. As channeling directions were avoided in the experiments, it is likely that trajectories close to $\alpha = 90°$ contribute little to the experimental averaging. See a similar consideration in the work of Schleife *et al.* [26] for a proton moving in aluminum. In order to compare the simulations to the experimental data in more detail, a model of the distribution of projectile trajectories would be needed to calculate an average S_e for a particular velocity, which involves nontrivial assumptions on the actual trajectories in experimental settings. S_e gradually diminishes toward the minimum at $\alpha = 90°$, starting at around $\alpha = 50°–60°$ where a slight maximum appears, especially at low velocities.
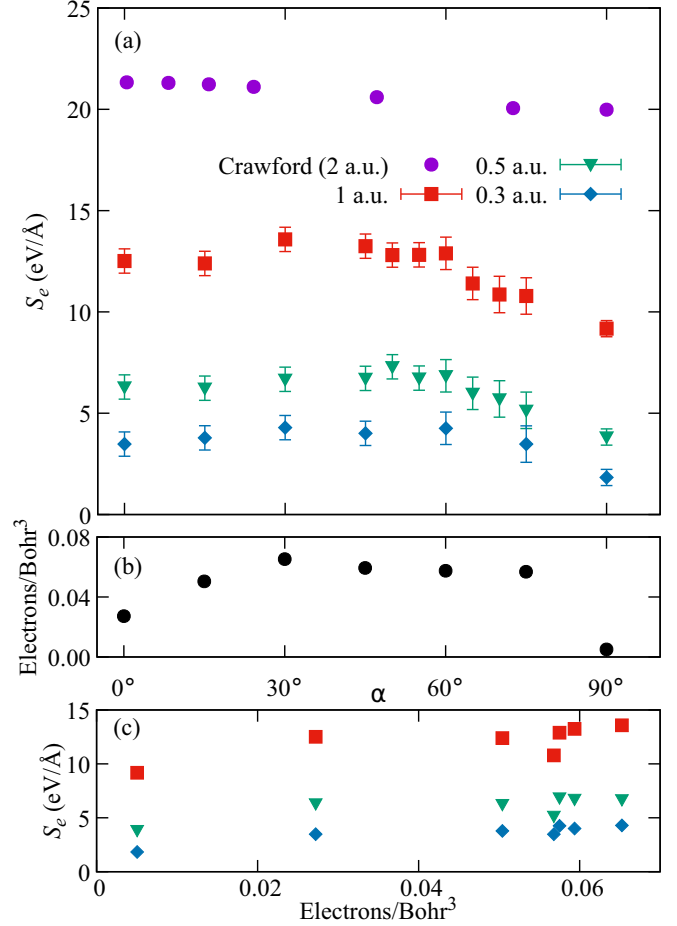

FIG. 4. (a) Electronic stopping power of a hydrogen atom in graphite moving at angle α from the graphite c axis at a velocity of 0.3, 0.5, and 1.0 a.u.. The data for 90° were calculated from simulations with the projectile moving midway between two planes of atoms along $\beta = 0°$ (see Figs. 1 and 2). The error bars are due to the uncertainty in fitting to the slope of the energy plot. (b) Average electron density along the trajectory of the projectile for different α values. (c) Correlation between local electron density and S_e.

B. Dependence on α

Figure 3 shows the expected overall linear dependence of S_e in the displayed velocity range, with a slow downward bending as velocity increases toward the S_e maximum related to the Bragg peak, which in graphite is at ∼1.9 a.u. [49]. The curve for $\alpha = 90°$ is clearly different, however, corresponding to trajectories parallel to graphitic planes. As Fig. 4 shows more clearly, the electronic stopping power decreases significantly at all velocities between $\alpha = 60°$ and 90°. The data for $\alpha = 90°$ correspond to the projectile moving midway between two planes of atoms along $\beta = 0°$ (see Figs. 1 and 2).

Figure 4 also includes the linear-response results of Crawford [9] for comparison. The lowest velocity considered in that work is $v = 2.0$ a.u., higher than those obtained in this work, which accounts for the higher overall S_e. They also show a smaller angle dependence, of approximately 10% between a projectile moving along $\alpha = 0°$ and 90° at 2 a.u., with smaller differences at higher projectile velocities, significantly lower than the equivalent difference for $v = 1.0$ a.u. in our case.

This is consistent with a further insensitivity with direction at high velocities [9]. Figure 9 of Shukri, Bruneval, and Reining's paper [10] also shows a small difference of up to 3% in S_e between calculations with a projectile moving along $\alpha = 0°$ and $90°$ in graphite at velocities between 0 and 4 a.u. As discussed below, that work calculated the random electronic stopping power, which is averaged over all impact parameters, and so is not directly equivalent to the results in this paper.

1. Correlation of S_e and electron density

Figure 4(b) shows the average electron density along a given trajectory versus α for comparison with $S_e(\alpha)$, with the correlation between the two plotted in Fig. 4(c). The relationship between the electron density and S_e is especially clear for the low velocities, with both S_e and electron density increasing from $\alpha = 0°$ to $30°$, and the lowest S_e at $90°$ corresponding to the lowest electron density.

Under the scattering theory formalism developed by Echenique and others for jellium [12,50–52], the target electron density is space independent, a number n, and the stopping power is a function $S_e(v, n)$, which starts at zero for $n = 0$ and increases with higher density. This result has been generalized to nonhomogeneous electron systems, with the observation that the stopping power is larger when the projectiles traverse regions of higher density. This has been seen in previous work in various materials [27,50–52], and is used as a basic assumption in different contexts, as a local-density stopping approximation [52]. The results of the simulations presented here are consistent with this; between the graphitic layers the electron density is much lower than across the layers, and the higher the angle of the projectile relative to the c axis the more time it spends in the lower electron density region between the layers. As a result, the projectile interacts less with the electrons of the target and so the S_e is lower, as seen in Fig. 4, obtaining the minimum S_e for $\alpha = 90°$ and the projectile moving midway between the planes, that is, the trajectory furthest from the carbon atoms and thus with the lowest electron density. It must be noted, however, that although the correlation is clear, it is not strict, as can be observed for $\alpha = 75°$, although because of the orientation within the cell, the sampled trajectory both for the evaluation of S_e and for the sampling of density values is poorer, which could be behind the larger deviation.

2. Channeling

The main channeling direction in graphite is along the c axis ($\alpha = 0°$), but the effect on S_e is limited. Only a small depression can be observed for S_e for $\alpha = 0°$ as compared with $15°$ at low velocity. In Fig. 4 it is visible for $v = 0.3$–0.5 a.u., but it is clearly a much smaller effect than the one for $\alpha = 90°$ (parallel to graphitic layers) even if using perfect channeling trajectories, as trajectory 1 in Fig. 1. These results are consistent with the previous discussion since the average density along that path does not reduce as much as for those parallel to and midway between graphitic planes.

Channeling in a crystal occurs when a projectile arrives into a channel in a trajectory within a small angle from the channel in a major crystal direction, and then moves along it

undergoing small-angle scattering, thereby moving along the channel. It is customarily expected that, as a result of the lack of nuclear collisions with the target material (beyond the small deflections implied by the channeling itself) and thereby reduced total energy loss of the projectile, the projectile travels further compared with a random direction in the crystal [53]. For light projectiles and velocities above ~ 0.1 a.u., however, that effect becomes less important than the fact that S_e itself is expected to be lower along a channeling direction, due to the lower average electron density in a channel; Schleife, Kanai, and Correa [26] carried out TDDFT simulations of H in Al, comparing projectiles moving along channels with off-channeling directions, and found lower S_e for a projectile moving along a channeling direction than along a random nonchanneling direction. Channeling in graphite has only been experimentally observed when the projectile is moving along the c axis of graphite, perpendicular to the graphitic layers [54–56]. That work used polycrystalline highly oriented pyrolytic graphite (HOPG), containing grain boundaries perpendicular to the graphitic layers, which would disrupt channeling between the layers. In HOPG, the basal planes are closely aligned, but alignment along the other axes is difficult to achieve. In theory, channeling would also be expected for a projectile traveling parallel to the graphitic layers, and the projectiles moving along $\alpha = 90°$ do show significantly lower S_e.

3. Low velocity

The behavior of S_e in the low-velocity end of Fig. 3 is remarkable. On the one hand, the simulations with the projectile moving at angles other than $90°$ to the c axis appear to show a threshold velocity of 0.02–0.06 eV below which, extrapolating the calculated data, S_e appears to be either zero or very small on that scale. This is consistent with behavior seen in insulators [27] where the band gap results in a velocity threshold for S_e. Graphite is effectively a semiconductor in the direction perpendicular to the graphitic layers, and, in that sense, this behavior would appear to be consistent with what is expected, at least qualitatively. In contrast, the obtained S_e shown in Fig. 3 for $\alpha = 90°$, corresponding to a projectile moving midway between the graphitic layers, displays a very different behavior, with no apparent threshold but rather $S_e \propto v$, but with a clear change of slope at $v \sim 0.3$ a.u. displayed by the lowest $S_e(v)$ graph in Fig. 3.

C. Protons traveling between graphitic planes

Figure 5 shows the behavior for trajectories parallel to the graphitic planes in more detail, with the $S_e(v)$ dependence for different orientations [Fig. 5(a)] and different impact parameters [proximity of the trajectory to the closest plane, Fig. 5(b)]. Starting with Fig. 5(a), as discussed above, the S_e is much lower at all velocities and all angles where the projectile is traveling parallel to the graphitic layers, as a result of the lower electron density between the layers. Due to the hexagonal symmetry of graphite, the trajectories $\beta = 0°$ and $60°$ are crystallographically identical. $S_e(\beta)$ should therefore be periodic with a period of $60°$. It is expected to be symmetric around $0°$ and $30°$, the values of S_e for those β's representing likely bounds for $S_e(\beta)$. Figure 5(a) shows S_e at 0 and $30°$ as
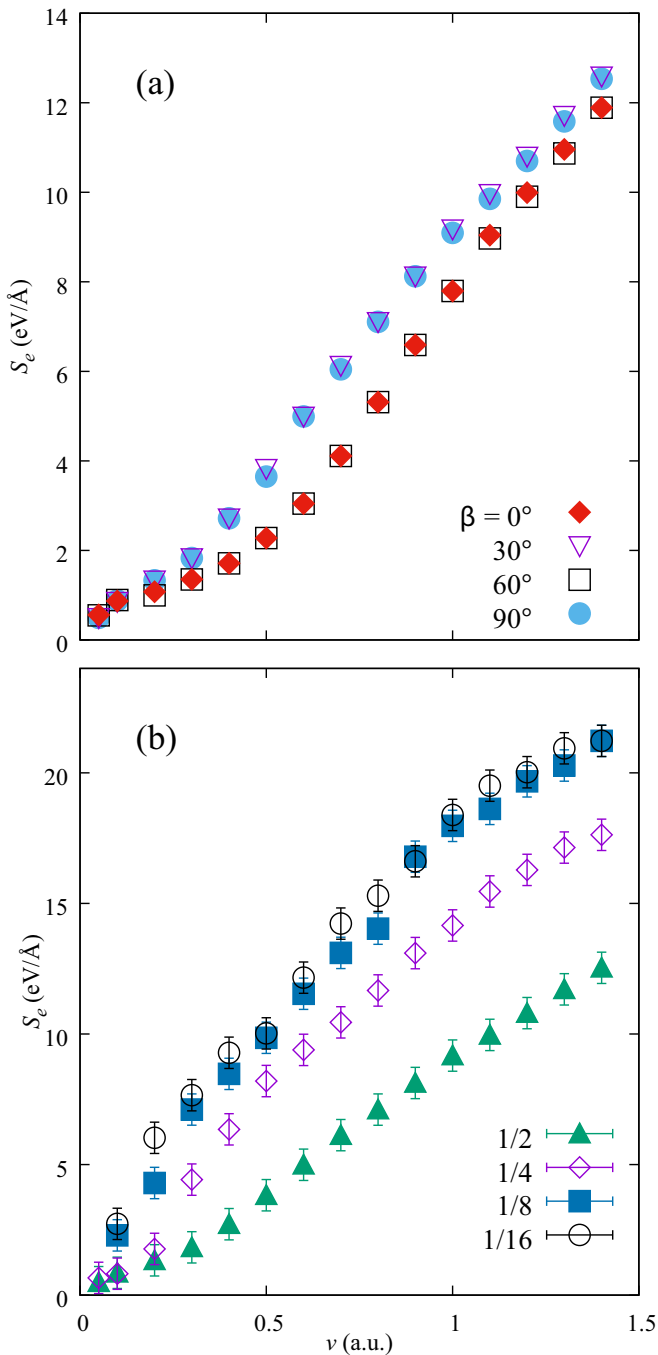
FIG. 5. (a) Shows the electronic stopping power for a projectile moving parallel to the graphitic layers at angles β from the a axis of graphite, midway between the graphitic layers. (b) Compares the electronic stopping power for a proton moving at different distances from the graphitic layers as a fraction of the interplanar distance (Fig. 2). The electronic stopping power increases the closer the path of the projectile is to a graphitic layer, likely due to the higher electron density closer to the planes.

a function of velocity. The periodicity has been checked with the inclusion of results for $\beta = 60°$ and $90°$.

Figure 5(a) shows that the change of slope remains apparent for trajectories equidistant from two graphitic planes, irrespective of the β angle, although for $\beta = 0°$ it happens at a slightly larger value of v ($v_K \sim 0.4$ a.u.) than for $\beta = 30°$

($v_M \sim 0.3$ a.u.). The former corresponds to the direction of the K point in reciprocal space, while the latter to the M-point direction. Both values are close to the Fermi velocity of electrons around the Dirac cone ($v_F = 0.37$ a.u.), indicating that the change of slope is due to the onset of intracone electron-hole transitions contributing to the stopping. We base this observation on the fact that the electron-hole excitations generated by the moving projectile should respect the relation [27]

$$\mathbf{v} \cdot \Delta \mathbf{k} = \Delta \epsilon,$$

being $\Delta \mathbf{k}$ and $\Delta \epsilon$ the momentum and energy change of the electron, respectively, in the excitation, and $\mathbf{v}$ the projectile's velocity. For $v < v_F$, excitations can only be connecting across cones, while for $v \gtrsim v_F$ the intracone channel is open.

A similar increase in the S_e gradient at velocities between 0.3 and 0.5 a.u. has been seen in experiments for various systems: protons in Au [57,58], He in Al [59], and protons and He in Cu [60], to name a few. The change in gradient for the Cu and Au experiments is suggested to be a result of interactions with the target's $3d$ and $5d$ electrons in Cu and Au, respectively, at higher projectile velocities, where a minimum energy transfer is required for the excitation of d electrons in both metals [57]. For He in Al, the slope change is thought to be due to charge-exchange processes between the target atoms and projectile [59]. This again suggests that the increase in gradient is due to additional energy loss mechanisms becoming accessible beyond a certain velocity, and which, in this case would correspond to the mentioned intracone transitions, meaning electron-hole-pair formation within the same band and small momentum transfer within the Brillouin zone, as the velocity approaches the Fermi velocity of the host.

Impact-parameter dependence

The impact-parameter dependence is shown in Fig. 5(b). It compares the S_e for a projectile moving midway between the graphitic layers, and at positions $\frac{1}{4}$, $\frac{1}{8}$, and $\frac{1}{16}$ of the interplanar distance from a graphitic layer, as shown in Fig. 2(b). The S_e is higher at all velocities above 0.1 a.u. for the simulations closer to the graphite atoms, corresponding to the higher electron density closer to the graphitic layer. The gradient of the S_e plot changes as the velocity increases, with a linear region between 0.5 and 1 a.u., and a slight decrease in gradient at higher velocities for both paths as the S_e approaches a maximum. When the trajectories get closer to either atomic plane [Fig. 5(b)], S_e significantly increases as compared to the midplane trajectory, and the clean two-slope structure of Fig. 5(a) is lost, which should be attributed to scattering amplitude effects.

Trajectories perpendicular to the graphitic planes do not display significant impact-parameter dependence, however, unlike what is seen for trajectories parallel to the planes. S_e increased only by 0.68 eV/Å when changing from trajectory 1 in Fig. 1 to trajectory 4 at $v = 0.5$ a.u.

The results of Shukri, Bruneval, and Reining [10] investigated random electronic stopping power, defined as the S_e averaged over all impact parameters. For the in-plane simulations, this is equivalent to averaging S_e for all the trajectories

at different distances from the graphitic layers. As Fig. 5 shows, there is a significant increase in S_e as the trajectory gets closer to a graphitic layer. The 3% difference between in-plane and out-of-plane simulations in S_e seen by Shukri *et al.* [10] is therefore consistent with the results in this work. Figure 3 shows the RESP from this work calculated as an average of the four impact parameters simulated for $\alpha = 90°$. This simple average oversamples trajectories close to the graphitic layers (higher S_e and therefore is an overestimate of the RESP; at high velocities we would expect all trajectories to be sampled equally).

IV. CONCLUSIONS

Simulations of a hydrogen projectile traveling through graphite successfully reproduced experimental results, and provided new insights into the effect of the anisotropy of the graphite structure on electronic stopping power. The electronic stopping power is dependent on the direction of the projectile both relative to the graphitic layer normal and parallel to the layers. Although a clear correlation is found between the local electron density traversed by the trajectory in general, at low velocity S_e displays varied behaviors depending on the direction and impact parameter. For channeling between planes and low density, a linear S_e is observed, consistent with (semi)metallic electron conduction, but which changes slope when the projectile velocity reaches the Fermi velocity of the target. For trajectories with dominant component perpendicular to the graphitic plane, a threshold is observed at $v \sim 0.05$ a.u., consistent with poor electron conduction between planes.

This work investigates the initial stages of radiation damage; for a fuller understanding of the processes that lead to the final observed radiation damage, simulations must be carried out at longer timescales and with larger simulation sizes. Progression from S_e calculations can be envisaged by following the diffusion of the excess electronic energy, and its thermalization to the ionic motion. In addition to the technical challenges from increased simulation size, theoretical challenges also exist, as Ehrenfest dynamics are known to be inadequate for the simulation of this thermalization. Beyond Ehrenfest approximations are far more computationally demanding, and therefore present a significant challenge but would offer valuable insights into the progress of stopping processes and the mechanisms of radiation damage.
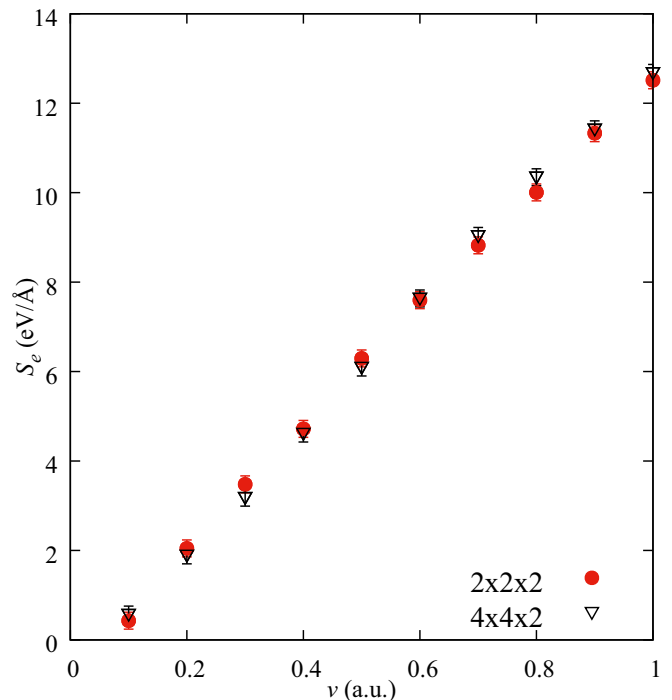
ACKNOWLEDGMENTS

FIG. 6. Comparison of electronic stopping power in graphite with a hydrogen projectile traveling at 0.1 to 1 a.u. with supercell sizes of $2 \times 2 \times 2$ and $4 \times 4 \times 2$ primitive unit cells. In these simulations, the projectile moved perpendicular to the graphitic planes along the shortest supercell dimension, through the center of a channel.

APPENDIX

This Appendix describes the testing carried out to generate the initial simulation parameters. The pseudopotentials of C and H were generated using the scheme of Troullier and Martins [40] and the corresponding parameters are shown in Table I.

Table II gives the parameters needed for the generation of the basis set used in this work, following the procedures described in Ref. [63]. The polarization orbitals were generated

TABLE I. Pseudopotential radii for each angular-momentum channel of C and H. Lengths are in bohrs.

Species	s	p	d	f
C ($2s^2 2p^2$)	1.49	1.50	1.56	1.56
H ($1s^2$)	1.25	1.25	1.25	1.25

TABLE II. Cutoff radii $r(\zeta_1)$ and $r(\zeta_2)$ in bohrs of the first and second ζ functions of C and H.

Species	n	l	$r(\zeta_1)$	$r(\zeta_2)$
C	2	0	4.192	3.432
	2	1	4.870	3.475
H	1	0	4.828	3.855

by applying an electric field to the orbital according to the procedure implemented in SIESTA and described in Ref. [37].

A periodic supercell of $2\times2\times2$ graphite unit cells was used, containing 32 C atoms and a single H atom, with lattice parameters of $a = 2.461$ Å, $c = 6.573$ Å. A number of supercell sizes were tested to confirm that the supercell used was sufficiently large to give good quality results. Figure 6 compares the electronic stopping power for a projectile moving perpendicular to the graphitic layers in $2\times2\times2$ and a $4\times4\times2$ supercells containing 33 and 129 atoms. There is no significant difference between the electronic stopping powers in this velocity range for the two supercell sizes, confirming that the $2\times2\times2$ supercell is sufficient to produce accurate results.

A single k point (Γ) was used for the Brillouin zone integrations, after testing a ground-state calculation with up to 90 k points for convergence and simulation time. The difference between S_e for one k point and 96, for trajectory number 1 and $v = 1$ a.u., was only 0.2 eV/Å. A time step of 1 attosecond was used for the low-velocity simulations up to 1 a.u., and of 0.1 attoseconds for simulations above 1 a.u. after testing for the stability of the Crank-Nicolson integrator algorithm and the energy change in a TDDFT simulation. The plane-wave energy cutoff for real-space integration was tested between 50 and 400 Ry; the total energy converged at around 150 Ry, and a 200 Ry cutoff energy was finally used in the simulations.

[1] G. S. Was, *Fundamentals of Radiation Materials Science* (Springer, Berlin, 2007).

[2] A. C. Begg, F. A. Stewart, and C. Vens, Nat. Rev. Cancer **11**, 239 (2011).

[3] F. H. Eisen, G. J. Clark, J. Bøttiger, and J. M. Poate, Radiat. Eff. **13**, 93 (1972).

[4] A. Dygo, M. A. Boshart, L. E. Seiberling, and N. M. Kabachnik, Phys. Rev. A **50**, 4979 (1994).

[5] J. H. R. dos Santos, P. L. Grande, M. Behar, H. Boudinov, and G. Schiwietz, Phys. Rev. B **55**, 4332 (1997).

[6] W. Käferböck, W. Rössler, V. Necas, P. Bauer, M. Peñalba, E. Zarate, and A. Arnau, Phys. Rev. B **55**, 13275 (1997).

[7] S. D. Softky, Phys. Rev. **123**, 1685 (1961).

[8] S. M. Seltzer and M. J. Berger, Int. J. Appl. Radiat. Isotopes **33**, 1189 (1982).

[9] O. H. Crawford, Phys. Rev. A **42**, 1390 (1990).

[10] A. A. Shukri, F. Bruneval, and L. Reining, Phys. Rev. B **93**, 035128 (2016).

[11] P. Echenique, R. Nieminen, and R. Ritchie, Solid State Commun. **37**, 779 (1981).

[12] P. M. Echenique, R. M. Nieminen, J. C. Ashley, and R. H. Ritchie, Phys. Rev. A **33**, 897 (1986).

[13] T. L. Ferrell and R. H. Ritchie, Phys. Rev. B **16**, 115 (1977).

[14] J. Lindhard, Mat. Fys. Medd. **28**, 1 (1954).

[15] P. Echenique, F. Flores, and R. Ritchie, Solid State Phys. **43**, 229 (1990).

[16] P. Sigmund, *Particle Penetration and Radiation Effects* (Springer, Cham, 2014), Vol. 2.

[17] D. R. Mason, J. le Page, C. P. Race, W. M. C. Foulkes, M. W. Finnis, and A. P. Sutton, J. Phys.: Condens. Matter **19**, 436209 (2007).

[18] C. P. Race, D. R. Mason, M. W. Finnis, W. M. C. Foulkes, A. P. Horsfield, and A. P. Sutton, Rep. Prog. Phys. **73**, 116501 (2010).

[19] A. V. Krasheninnikov, Y. Miyamoto, and D. Tománek, Phys. Rev. Lett. **99**, 016104 (2007).

[20] J. M. Pruneda, D. Sánchez-Portal, A. Arnau, J. I. Juaristi, and E. Artacho, Phys. Rev. Lett. **99**, 235501 (2007).

[21] M. A. Zeb, J. Kohanoff, D. Sánchez-Portal, A. Arnau, J. I. Juaristi, and E. Artacho, Phys. Rev. Lett. **108**, 225504 (2012).

[22] A. A. Correa, J. Kohanoff, E. Artacho, D. Sánchez-Portal, and A. Caro, Phys. Rev. Lett. **108**, 213201 (2012).

[23] M. A. Zeb, J. Kohanoff, D. Sánchez-Portal, and E. Artacho, Nucl. Instrum. Methods Phys. Res., Sect. B **303**, 59 (2013).

[24] A. Ojanperä, A. V. Krasheninnikov, and M. Puska, Phys. Rev. B **89**, 035120 (2014).

[25] A. Caro, A. A. Correa, A. Tamm, G. D. Samolyuk, and G. M. Stocks, Phys. Rev. B **92**, 144309 (2015).

[26] A. Schleife, Y. Kanai, and A. A. Correa, Phys. Rev. B **91**, 014306 (2015).

[27] R. Ullah, F. Corsetti, D. Sánchez-Portal, and E. Artacho, Phys. Rev. B **91**, 125203 (2015).

[28] M. Caro, A. A. Correa, E. Artacho, and A. Caro, Sci. Rep. **7**, 2045 (2017).

[29] S. Bubin, B. Wang, S. Pantelides, and K. Varga, Phys. Rev. B **85**, 235435 (2012).

[30] C.-W. Lee and A. Schleife, Eur. Phys. J. B **91**, 222 (2018).

[31] D. C. Yost, Y. Yao, and Y. Kanai, Phys. Rev. B **96**, 115134 (2017).

[32] D. D. L. Chung, J. Mater. Sci. **37**, 1475 (2002).

[33] J. Cazaux, Solid State Commun. **8**, 545 (1970).

[34] E. Yagi, T. Iwata, T. Urai, and K. Ogiwara, J. Nucl. Mater. **334**, 9 (2004).

[35] A. Tsolakidis, D. Sánchez-Portal, and R. M. Martin, Phys. Rev. B **66**, 235416 (2002).

[36] R. Ullah, A. Garaizar, F. Corsetti, J. Kohanoff, D. Sanchez-Portal, and E. Artacho (unpublished).

[37] J. M. Soler, E. Artacho, J. D. Gale, A. García, J. Junquera, P. Ordejón, and D. Sánchez-Portal, J. Phys.: Condens. Matter **14**, 2745 (2002).

[38] E. Artacho, E. Anglada, O. Diéguez, J. D. Gale, A. García, J. Junquera, R. M. Martin, P. Ordejón, J. M. Pruneda, D. Sánchez-Portal, and J. M. Soler, J. Phys.: Condens. Matter **20**, 064208 (2008).

[39] S. Froyen, N. J. Troullier, J. L. Martins, L. C. Balbás, J. M. Soler, and A. Garcia, ATOM, a program for DFT calculations in atoms and pseudopotential generation, https://departments.icmab.es/leem/siesta/Pseudopotentials/Code/downloads.html

[40] N. Troullier and J. L. Martins, Phys. Rev. B **43**, 1993 (1991).

[41] R. Ullah, E. Artacho, and A. A. Correa, Phys. Rev. Lett. **121**, 116401 (2018).

[42] D. M. Ceperley and B. J. Alder, Phys. Rev. Lett. **45**, 566 (1980).

[43] J. P. Perdew and A. Zunger, Phys. Rev. B **23**, 5048 (1981).

[44] W. Kohn and L. J. Sham, Phys. Rev. **140**, A1133 (1965).

[45] E. Runge and E. K. U. Gross, Phys. Rev. Lett. **52**, 997 (1984).

[46] W. Pietsch, U. Hauser, and W. Neuwirth, Nucl. Instrum. Methods **132**, 79 (1976).

[47] J. K. Tomfohr and O. F. Sankey, Phys. Status Solidi B **226**, 115 (2001).

[48] E. Artacho and D. D. O'Regan, Phys. Rev. B **95**, 115155 (2017).

[49] J. Deasy, Med. Phys. **21**, 709 (1994).

[50] N.-P. Wang, I. Nagy, and P. M. Echenique, Phys. Rev. B **58**, 2357 (1998).

[51] N.-P. Wang and I. Nagy, Phys. Rev. A **56**, 4795 (1997).

[52] H. Winter, J. I. Juaristi, I. Nagy, A. Arnau, and P. M. Echenique, Phys. Rev. B **67**, 245401 (2003).

[53] J. Lindhard, Mat. Fys. Medd. **34**, 1 (1965).

[54] B. S. Elman, G. Braunstein, M. S. Dresselhaus, G. Dresselhaus, T. Venkatesan, and B. Wilkens, J. Appl. Phys. **56**, 2114 (1984).

[55] T. Iwata, K.-I. Komaki, H. Tomimitsu, K. Kawatsura, K. Ozawa, and K. Doi, Radiat. Eff. **24**, 63 (1975).

[56] D. Schroyen, M. Bruggeman, I. Dezsi, and G. Langouche, Nucl. Instrum. Methods Phys. Res., Sect. B **15**, 341 (1986).

[57] E. A. Figueroa, E. D. Cantero, J. C. Eckardt, G. H. Lantschner, J. E. Valdés, and N. R. Arista, Phys. Rev. A **75**, 010901(R) (2007).

[58] S. N. Markin, D. Primetzhofer, S. Prusa, M. Brunmayr, G. Kowarik, F. Aumayr, and P. Bauer, Phys. Rev. B **78**, 195122 (2008).

[59] D. Primetzhofer, S. Rund, D. Roth, D. Goebl, and P. Bauer, Phys. Rev. Lett. **107**, 163201 (2011).

[60] S. N. Markin, D. Primetzhofer, M. Spitz, and P. Bauer, Phys. Rev. B **80**, 205105 (2009).

[61] http://www.hpc.cam.ac.uk

[62] www.dirac.ac.uk

[63] J. Junquera, O. Paz, D. Sánchez-Portal, and E. Artacho, Phys. Rev. B **64**, 235111 (2001).